Molecular Neurobiology (2019) 56:2653–2669
https://doi.org/10.1007/s12035-018-1235-1

Loss of Brain Norepinephrine Elicits Neuroinflammation-Mediated Oxidative Injury and Selective Caudo-Rostral Neurodegeneration

Sheng Song[1] · Lulu Jiang[1,2] · Esteban A. Oyarzabal[1,3] · Belinda Wilson[1] · Zibo Li[3] · Yen-Yu Ian Shih[3] · Qingshan Wang[1,4] · Jau-Shyong Hong[1]

Received: 29 March 2018 / Accepted: 10 July 2018 / Published online: 27 July 2018

Abstract

Environmental toxicant exposure has been strongly implicated in the pathogenesis of Parkinson's disease (PD). Clinical manifestations of non-motor and motor symptoms in PD stem from decades of progressive neurodegeneration selectively afflicting discrete neuronal populations along a caudo-rostral axis. However, recapitulating this spatiotemporal neurodegenerative pattern in rodents has been unsuccessful. The purpose of this study was to generate such animal PD models and delineate mechanism underlying the ascending neurodegeneration. Neuroinflammation, oxidative stress, and neuronal death in mice brains were measured at different times following a single systemic injection of lipopolysaccharide (LPS). We demonstrate that LPS produced an ascending neurodegeneration that temporally afflicted neurons initially in the locus coeruleus (LC), followed by substantia nigra, and lastly the primary motor cortex and hippocampus. To test the hypothesis that LPS-elicited early loss of noradrenergic LC neurons may underlie this ascending pattern, we used a neurotoxin N-(2-chloroethyl)-N-ethyl-2-bromobenzylamine (DSP-4) to deplete brain norepinephrine. DSP-4 injection resulted in a time-dependent ascending degenerative pattern similar to that generated by the LPS model. Mechanistic studies revealed that increase in nicotinamide adenine dinucleotide phosphate (NADPH) oxidase-2 (NOX2)-dependent superoxide/reactive oxygen species (ROS) production plays a key role in both LPS- and DSP-4-elicited neurotoxicity. We found that toxin-elicited chronic neuroinflammation, oxidative neuronal injuries, and neurodegeneration were greatly suppressed in mice deficient in NOX2 gene or treated with NOX2-specific inhibitor. Our studies document the first rodent PD model recapturing the ascending neurodegenerative pattern of PD patients and provide convincing evidence that the loss of brain norepinephrine is critical in initiating and maintaining chronic neuroinflammation and the discrete neurodegeneration in PD.

Keywords Parkinson's diseases · Progressive neurodegeneration · Chronic neuroinflammation · Norepinephrine depletion · Oxidative and nitrosylative neuronal injuries

Sheng Song, Lulu Jiang, and Esteban A. Oyarzabal have equal contribution.

Electronic supplementary material The online version of this article (https://doi.org/10.1007/s12035-018-1235-1) contains supplementary material, which is available to authorized users.

✉ Qingshan Wang
wangq4@126.com

✉ Jau-Shyong Hong
hong3@niehs.nih.gov

[1] Neuropharmacology Section, Neurobiology Laboratory, National Institute of Environmental Health Sciences, National Institutes of Health, P.O. Box 12233, Mail Drop F1-01Research Triangle Park, North Carolina 27709, USA

[2] Institute of Toxicology, School of Public Health, Shandong University, Jinan, Shandong, China

[3] Biomedical Research Imaging Center, University of North Carolina at Chapel Hill, Chapel Hill, NC, USA

[4] Department of Toxicology, School of Public Health, Dalian Medical University, Dalian, Liaoning, China

Abbreviations

3-NT	3-nitrotyrosine
4-HNE	4-hydroxy-2-nonenal
CPu	caudate-putamen
CD11b	integrin αM chain
DA	dopamine
DAMPs	danger-associated molecular patterns
DHE	dihydroethidium
DPI	diphenyleneiodonium
DSP-4	N-(2-chloroethyl)-N-ethyl-2-bromobenzylamine
FDG	fludeoxyglucose
Hip	hippocampus
Iba-1	ionized calcium-binding adapter molecule-1
LC	locus coeruleus
LPS	lipopolysaccharide
MCtx	motor cortex
NE	norepinephrine
NeuN	neuronal nuclei
NOX2	nicotinamide adenine dinucleotide phosphate (NADPH) oxidase-2
PBR	peripheral benzodiazepine receptor
PET	positron emission tomography
ROS	reactive oxygen species
SN*pc*	substantia nigra *pars compacta*
SUV	standard uptake value
TH	tyrosine hydroxylase
TSPO	translocator protein
VTA	ventral tegmental area

Introduction

Parkinson's disease is an age-associated neurodegenerative disorder that progresses through several decades. The hallmark movement symptoms of Parkinson's disease are produced by the loss of dopaminergic neurons in the substantia nigra *pars compacta* (DA-SN*pc*), while neurodegeneration outside the basal ganglia produces mood changes [1, 2], cognitive impairment [3–6], anosmia [7], and gastrointestinal issues [8]. Though assessment of neurodegeneration outside the basal ganglia varies greatly among individuals with Parkinson's disease [9], retrospective studies have associated parkinsonian symptom severity with caudo-rostral degeneration of discrete neuronal populations [9–13]. While many genetic and environmental factors are thought to contribute to Parkinson's disease, the mechanism behind the caudo-rostral progression and neurodegeneration in Parkinson's disease remains unknown.

Many groups have postulated that "prion-like" transmission and propagation of α-synuclein along functionally connected neurons may explain the spatiotemporal pattern of progression and neurodegeneration. In support of this hypothesis, α-synuclein inclusions populate the brain in a caudo-rostral order known as Braak stages that begins in neuronal terminals of the olfactory bulb and gut and spreads to the dorsal motor nucleus of the vagus before ascending through the hindbrain, midbrain, and forebrain structures into higher-order cortical centers in parkinsonian brains [14]. However, the involvement of α-synuclein variants in neurodegeneration has been inconsistent in animal studies [15–17], suggesting that α-synuclein may be necessary but not sufficient in the progression of neurodegeneration in Parkinson's disease. We previously reported that chronic neuroinflammation induced by a single systemic injection of the bacterial endotoxin lipopolysaccharide in mice was sufficient to produce degeneration of the dopaminergic neurons in the substantia nigra pars compacta with motor deficits [18–20]. The main purpose of this study was to extend this finding and investigate whether chronic neuroinflammation is a principal factor producing discrete caudo-rostral patterns of neurodegeneration in Parkinson's disease.

In this study, we first assessed whether lipopolysaccharide (LPS)-induced chronic neuroinflammation could recapitulate the spatiotemporal order of neurodegeneration in Parkinson's disease. Interestingly, a discrete caudo-rostral pattern of neurodegeneration was observed in LPS-injected mice; loss of neurons was first detected in noradrenergic locus coeruleus (NE-LC) neurons, followed by DA-SN*pc* neurons, and finally hippocampus and primary motor cortex. The finding showing early loss of NE-LC neurons in LPS-injected mice prompted us to further investigate the role of brain NE in modulating the susceptibility of neurons in regions innervated by NE-LC neurons. We hypothesized that an early loss of NE-LC neurons in Parkinson's disease may disrupt microglial immunohomeostasis to generate neuroinflammation and lead to neurodegeneration [21–24], similar to that observed following LPS injection. To test this possibility, we used a neurotoxicant N-(2-chloroethyl)-N-ethyl-2-bromobenzylamine (DSP-4) to selectively deplete central norepinephrine in NE-LC neurons. Consistent with our speculation, depletion of central norepinephrine produced discrete oxidative and nitrosylative neuronal injuries and degeneration along the predicted spatiotemporal order similar to that observed in LPS-treated mice. Results from both LPS and DSP-4 studies further emphasize the essential role of chronic neuroinflammation as a common driving factor in causing the neurodegeneration. Finally, the critical role of nicotinamide adenine dinucleotide phosphate (NADPH) oxidase-2 (NOX2) in the generation and maintenance of DSP-4-induced chronic neuroinflammation was substantiated in mice with genetically ablated CYBB gene coding for NOX2 or pharmacological inhibition of NOX2. Together, this study offers new insight into the critical role of NE-LC neurons in driving neurodegeneration in Parkinson's disease. This animal model is the first to show that early loss of central norepinephrine from the loss of NE-LC neurons is critical in

dysregulation of microglia throughout the brain to induce chronic neuroinflammation that afflicts the most vulnerable neuronal populations to produce the spatiotemporal pattern of neurodegeneration associated with Parkinson's disease.

Materials and Methods

Animals and Exposure Models

C57BL/6J and gp91$^{phox-/-}$ mice were obtained from the Jackson Laboratory (Bar Harbor, ME) and maintained in a 12-h light/dark cycle with *ab lib* access to food and water. All procedures were in strict accordance with the NIH animal welfare guidelines. Three-month-old male mice were exposed to either a single intraperitoneal injection of the bacterial endotoxin LPS (Sigma-Aldrich, L3012, 15×10^6 EU/kg), the norepinephrine-depleting neurotoxin DSP-4 (Sigma-Aldrich, C8417, 50 mg/kg), or a saline vehicle (5 ml/kg). Coronal-sectioned brain slices were used to assess neurodegeneration at 1, 4, 7, and 10 months following injections ($n = 6$–8/group) to determine whether exposures could initiate progressive caudo-rostral neurodegeneration. gp91$^{phox-/-}$ transgenic mice incapable of NOX2 activation and producing superoxide were treated with DSP-4 and assessed at 4 months following injection to examine whether NOX2 activation during neuroinflammation drives neurodegeneration. Wild-type mice (C57/BL) were subjected to subcutaneous implants of osmotic mini-pumps that infuse 10 ng/kg/day of the NOX2 inhibitor diphenyleneiodonium (DPI) for three months beginning a month after DSP-4 injection and assessed at four months after injection. All mice were euthanized by pentobarbital overdose and cardiac perfusion prior to excising their brains, post-fixation with 4% paraformaldehyde at 4 °C for 48 h, and subsequently infiltrated with 30% sucrose in PBS prior to sectioning.

Immunohistochemistry and Stereological/Automated Counting Assessments of Neurodegeneration

Free-floating 35 μm coronal sections containing the LC, SN*pc*, VTA, hippocampus (Hip), motor cortex (MCtx), and caudate putamen (CPu) were cut on a horizontal sliding microtome. Noradrenergic neurons of the LC and dopaminergic neurons of the VTA and SN*pc* were identified through TH$^+$ immunohistochemistry, whereas the pan-neuronal marker NeuN was used to identify all neurons in the Hip, MCtx, and CPu. Stereological counts of TH$^+$ LC, VTA, and SN*pc* neurons were estimated using an optical fractionator method on an Olympus BX50 stereological microscope within user-defined boundaries [20]. Automated counting was performed on high-density clusters of NeuN$^+$ neurons in the Hip, MCtx, and CPu, which was performed using an automated counting feature on ImageJ [25]. All immunohistochemistry images were captured by a Leica Aperio AT2 scanner.

PET Imaging of Glucose Metabolism to Assess Neurodegeneration

Regional differences in [^{18}F]-fludeoxyglucose (FDG) tracer accumulation is a widely-used clinical technique that quantifies changes in local cerebral metabolic rates of glucose that are suppressed in neurodegenerative disorders [26–28]. Mice underwent [^{18}F]-FDG positron emission tomography (PET), and the radiotracer accumulation was mapped in standardized uptake values (SUVs) and quantified by brain region using a mouse [^{18}F]-FDG atlas [29] and the software package AMIRA (v5.2, FEI).

Immunohistochemistry and Densitometry Assessments of Reactive Microgliosis

Reactive microgliosis was assessed in the SN*pc*, Hip, MCtx, and CPu by immunohistochemistry using either a polyclonal rabbit antibody against Iba-1 (Wako, 019-19741, 1:5000) or a monoclonal rat antibody against CD11b (AbD Serotec, MCA711G, 1:400). Densitometry of Iba-1$^+$ or CD11b$^+$ expression by microglial was assessed in the substantia nigra (SN), Hip, and MCtx using ImageJ as reported previously [30].

Autoradiography and PET Assessment of Neuroinflammation

Recent clinical PET imaging studies have implemented the binding of the radioligand [^{18}F]-peripheral benzodiazepine receptor (PBR) to mitochondrial transmembrane proteins (TSPO) selectively upregulated in immunologically activated microglia and astrocytes as a functional marker for neuroinflammation. The specificity of the ligand was validated by performing autoradiography of the radioligand and overlaying it with the immunohistochemistry detecting reactive microgliosis on the same sections. [^{18}F]-PBR-111 uptake was measured in vivo with PET imaging, and standardized uptake values were extracted from several brain regions to evaluate neuroinflammation.

In Situ and Immunohistochemistry Assessments of ROS and Oxidative and Nitrosylative Injuries

Coronal sections of the SN*pc*, MCtx, and the DG, CA1, CA2, and CA3 layers of the hippocampus were assessed for elevated superoxide/reactive oxygen species (ROS) production through an in situ method. Dihydroethidium (DHE, 20 mg/kg; i.p.) was injected to living mice 18 h before whole-body

perfusion. DHE that entered the brain was oxidized by superoxide and other oxidative radicals to form red fluorescent metabolites. Oxidative and nitrosylative cellular injuries were assessed by immunohistochemistry for 4-hydroxy-2-nonenal (4-HNE) lipid peroxidation adducts and 3-nitrotyrosine (3-NT) protein adducts, respectively. Densitometry was performed using ImageJ.

Statistical Analysis

All group data are expressed as mean ± SEM. Group means were compared using one- or two-way ANOVA with treatments as the independent variable, and statistical significance was defined at an alpha level of 0.05. Pairwise comparisons between group means were examined using the Dunnett's post-hoc test among groups with significant differences. Statistical analyses were performed on Prism (GraphPad, v7.00).

Additional methods are provided in the Supplementary Material.

Results

LPS-Induced Chronic Neuroinflammation Drives Progressive Neurodegeneration

We previously reported that a single LPS injection in mice produces parkinsonian-like neurodegeneration of DA-SN*pc* neurons with motor deficits [18], yet neurodegeneration outside the basal ganglia was not assessed in this model. Immunostaining of six discrete brain neuronal populations revealed that the earliest neurodegeneration occurred in TH^+ NE-LC neurons after LPS injection, which is similar to the early loss of NE-LC neurons observed in some Parkinson's disease patients. Significant NE-LC neurodegeneration was observed at 4, 7, and 10 months following LPS injection with 27 ± 1.8% ($p = 0.009$), 42 ± 2.6% ($p < 0.001$), and 54 ± 2.1% ($p < 0.001$) losses when compared to neuronal counts in age-matched vehicle controls (Fig. 1a,b). Analogous to the progression of neurodegeneration during Parkinson's disease, significant loss of TH^+ DA-SN*pc* neurons trailed the loss of NE-LC neurons by 3 months, becoming significant by 7 months (34 ± 2.1%, $p = 0.001$) and 10 months (50 ± 3.0%, $p < 0.001$) following LPS injection (Fig. 1a,b). Significant losses were observed in $NeuN^+$ neurons in the MCtx preferentially afflicted layers I, V, and VI (28 ± 0.9%, $p < 0.001$) and the hippocampal dentate gyrus (30 ± 1.2%, $p < 0.001$; Fig. 1a,b) by 10 months following LPS injection. Loss of neurons in these regions may correspond to the development of cognitive impairments, dementia, and psychosis at late stages of Parkinson's disease. By contrast, similar to the findings from parkinsonian patients [31, 32], the numbers of intrinsic $NeuN^+$ neurons in the CPu and TH^+ DA neurons in the VTA were not significantly affected up to10 months following LPS injection (Fig. 1a,b).

To further validate the spatial pattern of neurodegeneration, we assessed [^{18}F]-FDG uptake by in vivo whole-brain PET imaging to identify brain regions with depressed cerebral metabolic rates of glucose to detect regions of neurodegeneration. Significant suppression in glucose metabolism was observed by 10 months following LPS-induced chronic neuroinflammation by 28 ± 1.1% in the hindbrain ($p = 0.01$), midbrain by 28 ± 0.6% ($p = 0.02$), hippocampus by 23 ± 0.7% ($p = 0.02$), and across all cerebral cortices by 16 ± 1.0% ($p = 0.01$) when compared to basal metabolic levels of the vehicle control cohort (Fig. 1c,d). Furthermore, significant reductions in glucose metabolism were observed in the cerebellum (9 ± 0.8%, $p = 0.01$), olfactory bulb (22 ± 0.6%, $p = 0.01$), and thalamus (27 ± 0.7%, $p = 0.01$; Fig. 1c,d). By contrast, glucose metabolism was unchanged in the CPu ($p = 0.21$). Taken together, it appears that LPS-induced reductions in glucose metabolism and neurodegeneration in various brain regions are well-correlated.

The intensity of microglia activation may contribute largely to the rate of collateral neurodegeneration [33]. To determine microglial activation in different regions of the brain, we first assessed the intensity of microgliosis by immunostaining CD11b antigen, which is a selective marker for microglia, in sagittal sections of brains 10 months following injection of either LPS or a vehicle control. Results indicated clear enhancement of CD11b immunoreactivity in the MCtx, Hip, SN, and LC, with the exception of the caudate/putamen (CPu), which showed little change (Fig. 2a). Results from Figs. 1a and 2a suggest a high degree of correlation among the brain regions, which display enhanced immunostaining CD11b and neuronal loss in LPS-injected mice.

Next, we employed [^{18}F]-PBR-111 as a tool to further characterize the activation of microglia after LPS injection. Functional maps of immunologically activated microglia can be generated by PET imaging by determining the selective uptake of [^{18}F]-PBR-111 in Parkinson's disease patients [26]. We first performed autoradiography of [^{18}F]-PBR-111 and immunostaining of $CD11b^+$ microglia on the same sections to verify the cell type. Results showed that the increase of uptake of [^{18}F]-PBR-111 correlated well with the activated microglia (Fig. 2b). Uptake of [^{18}F]-PBR-111 by PET imaging in mice at 10 months following LPS injection was significantly elevated in the cerebellum (81 ± 8.5%, $p < 0.001$), hindbrain (88 ± 9.5%, $p < 0.001$), midbrain (168 ± 8.4%, $p < 0.001$), hippocampus (147 ± 8.6%, $p < 0.001$), thalamus (194 ± 6.7%, $p < 0.001$), and across the entire cerebral cortex (267 ± 13.2%, $p < 0.001$) with much less increase in caudate/putamen (31 ± 2.4%, $p = 0.04$) when compared to age-matched vehicle controls (Fig. 2c,d).

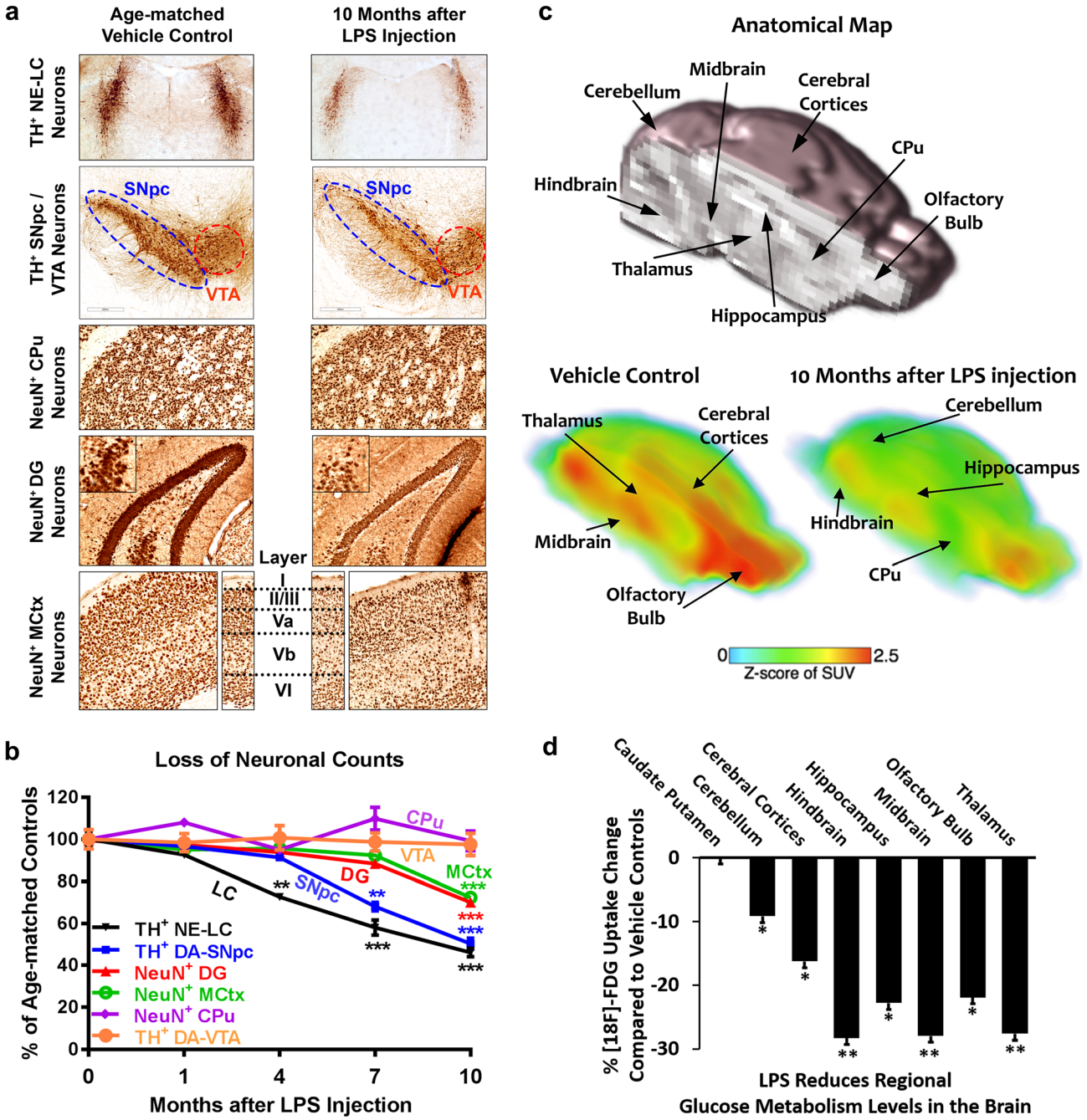

Fig. 1 Chronic neuroinflammation generated by a single LPS injection (15×10^6 EU/kg; i.p.) was sufficient to generate discrete, progressive neurodegeneration resembling the spatiotemporal pattern of neurodegeneration in Parkinson's disease. We assessed neurodegeneration in percent neuronal loss compared to stereological counts of age-matched vehicle controls at 1, 4, 7, and 10 months following LPS injection ($n = 4$–6/group). **a** Representative immunostaining images show TH-positive noradrenergic neurons in locus coeruleus (LC), dopaminergic neurons in substantia nigra *pars compacta* (SN*pc*) and ventral tegmental area (VTA), and NeuN-positive neurons in caudate/putamen (CPu), dentate gyrus (DG), and motor cortex (MCtx) at 10 months following LPS or saline vehicle injections. The stereological counting number of TH+ DA neurons in the SNpc of saline and LPS-treated mice is 6859 ± 278 and 4078 ± 206. Bar = 300 μm. **b** Neurodegeneration following LPS injection was sequentially observed to occur at NE-LC, DA-SN*pc*, DG, and MCtx neurons while sparing DA-VTA and CPu neurons. **c** Upper panel shows the anatomical orientation and brain regions for all PET maps. Lower panels are averaged whole-brain [^{18}F]-FDG PET maps ($n = 4$/group) of mice at 10 months following exposures to vehicle control (left) and LPS (right). LPS results in brain-wide reductions in glucose metabolism. Warmer colors represent increases in the *Z* score of [^{18}F]-FDG standard uptake values. **d** Quantification of standard uptake value changes among different brain regions following LPS injection displayed as percent reduction from vehicle control uptake. Data are expressed as mean ± SEM. * denotes $p < 0.05$, ** $p < 0.01$, and *** $p < 0.001$

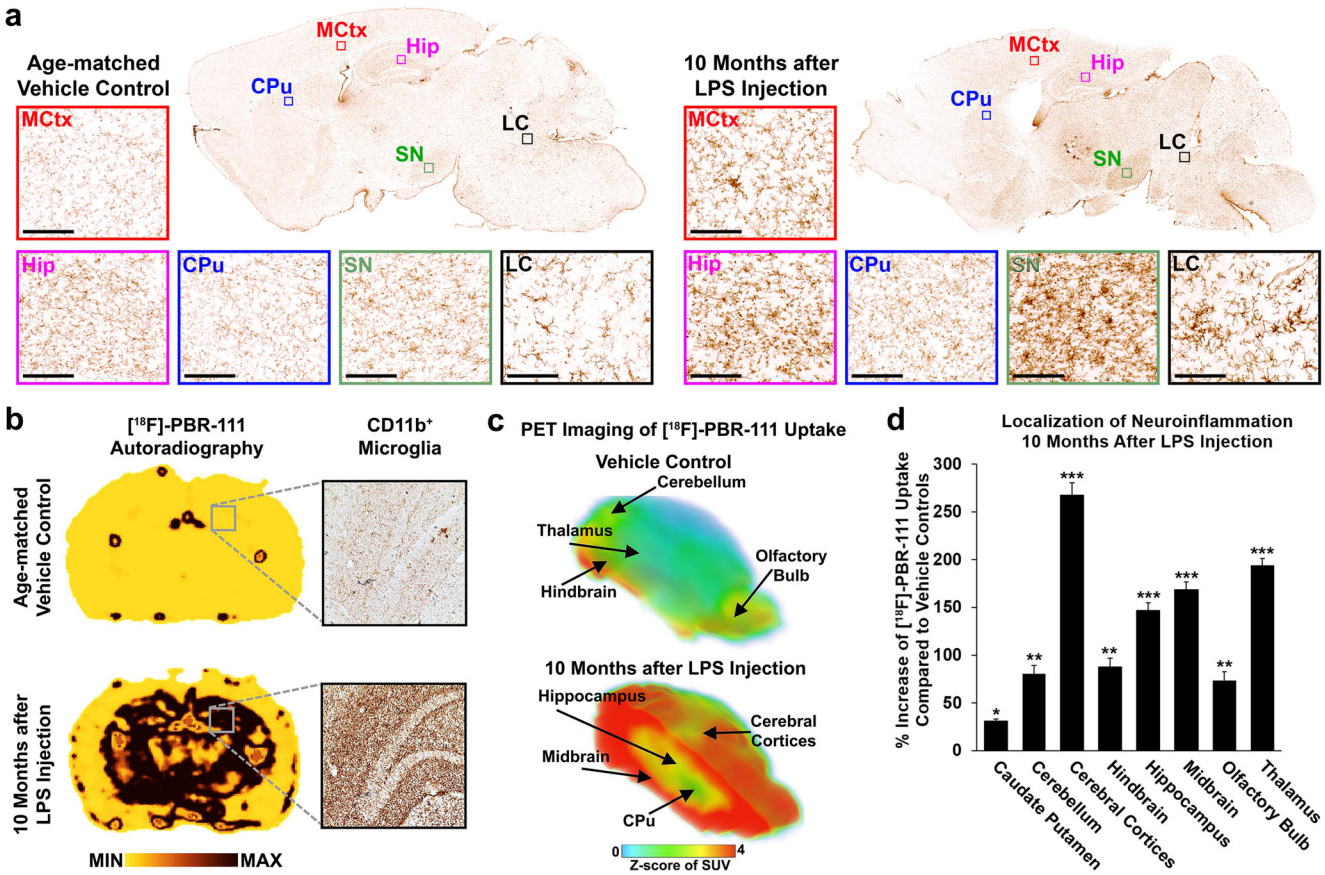

Fig. 2 LPS induces chronic neuroinflammation with heterogeneous densities of microgliosis across several brain regions associated with neurodegeneration in Parkinson's disease. **a** Representative immunostaining images of CD11b$^+$ microglia of sagittal sections from mice at 10 months following exposures to vehicle control (left) and LPS (right). Panels show immunostaining images with increased magnification in the motor cortex (MCtx), hippocampus (Hip), caudate/putamen (CPu), substantia nigra (SN), and locus coeruleus (LC). Scale bar = 60 μm. **b** Representative autoradiography of [^{18}F]-PBR-111 uptake corresponds to matching CD11b$^+$ immunostaining images on the same coronal section and confirms that change in radioligand uptake is dependent on microglia density. [^{18}F]-PBR-111 accumulation detected in age-matched vehicle controls seems to form in ventricles, likely detecting excretion of the radioligands into the cerebral spinal fluid. **c** In vivo PET imaging of [^{18}F]-PBR-111 uptake is detectable in the olfactory bulb and the hindbrain of age-matched vehicle controls and becomes significant throughout most of the brain with exception in the caudate/putamen. **d** Quantification of [^{18}F]-PBR-111 uptake is expressed as percentage increase in standard uptake values among different brain regions following LPS injection compared to vehicle control counterparts ± SEM. * denotes $p < 0.05$, ** $p < 0.01$, and *** $p < 0.001$

Depletion of Brain Norepinephrine by DSP-4 Elicits Progressive Neurodegeneration

In LPS-injected mice, brain regions showing neuronal loss are heavily innervated by noradrenergic nerve fibers with the exception of the caudate/putamen, which receive little noradrenergic innervation. The early loss of NE-LC neurons following an LPS injection led us to speculate that depletion of central norepinephrine from degeneration of NE-LC neurons may contribute to progressive neurodegeneration in the LPS model and even possibly in Parkinson's disease. To test this possibility, we injected mice with the neurotoxin DSP-4 to selectively deplete central norepinephrine. At different time points after DSP-4 injection, tissue extracts from different brain regions were prepared for the determination of tissue levels of norepinephrine by a high-performance liquid chromatograph analysis. Significant decrease of tissue levels of norepinephrine was observed one day after DSP-4 injection with losses of 55 ± 1.6% in the midbrain ($p < 0.001$), 70 ± 4.3% in the motor cortex ($p < 0.001$), and 78 ± 2.7% in the hippocampus ($p < 0.001$). Brain norepinephrine levels remained significantly reduced for up to 4 months. However, reduced levels of norepinephrine returned to normal values by 10 months post-injection (Fig. 3a). This observation suggests that DSP-4 temporarily suppresses the production of norepinephrine, but it does not cause loss of NE-LC. This finding is in line with the previous studies indicating that DSP-4 injection can alter TH expression without actually killing TH+ NE-LC neurons [34].

DA-SN*pc* neurons degenerated by 27 ± 2.5% ($p = 0.009$), 35 ± 1.4% ($p = 0.002$), and 53 ± 1.5% ($p < 0.001$) at 4, 7, and 10 months following DSP-4 injection, respectively, when

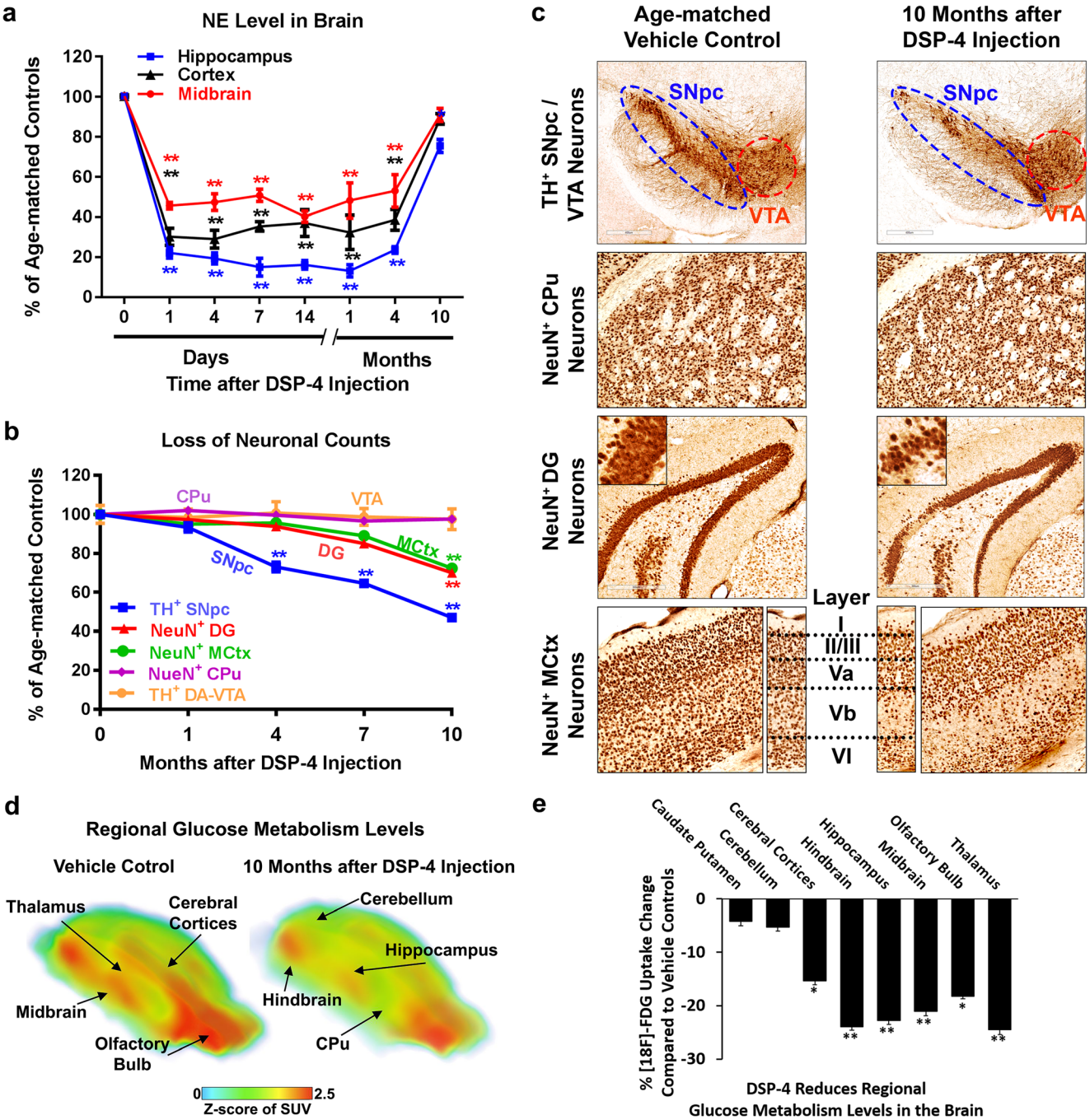

Fig. 3 A single systemic injection of DSP-4 (50 mg/kg, i.p.) induced progressive neurodegeneration resembling the spatiotemporal pattern observed in Parkinson's disease. **a** DSP-4 significantly reduced vesicular NE levels (measured by HPLC) in the midbrain, hippocampus (Hip), and motor cortex (MCtx). Results are expressed as percent reduction compared with age-matched vehicle controls (mean ± SEM; $n = 5–6$ mice/group). **b** Stereological counts were performed to determine percent neurodegeneration following DSP-4 injection; data were calculated compared to age-matched vehicle controls at 1, 4, 7, and 10 months following injection ($n = 4–6$/group). DSP-4 injection resulted in sequentially neurodegeneration in dopaminergic substantia nigra *pars compacta* (DA-SN*pc*), dentate gyrus (DG), and MCtx neurons while sparing caudate/putamen (CPu) and VTA neurons. The stereological counting number of TH+ DA neurons in the SNpc of saline- and DSP-4-treated mice is 6859 ± 278 and 3893 ± 176. **c** Representative immunostaining images show TH^+ NE-LC and DA-SN*pc*/VTA neurons and $NeuN^+$ CPu, DG, and MCtx neurons at 10 months following vehicle and DSP-4. Bar = 300 μm. **d** Reductions in regional glucose metabolism levels are observed in mice at 10 months following DSP-4 injection in averaged whole-brain [^{18}F]-FDG PET maps ($n = 4$/group) compared to age-matched vehicle controls. [^{18}F]-FDG standard uptake values were extracted for each brain region and normalized among subject using *Z* score transformation. Warmer colors represent brain regions with higher glucose uptake. **e** Brain region-specific changes in standard uptake values following DSP-4 injection were expressed as percent uptake reduction compared to vehicle controls. Data are expressed as mean ± SEM. * denotes $p < 0.05$ and ** $p < 0.01$

compared to age-matched vehicle controls (Fig. 3b,c). DSP-4 injection also resulted in NeuN$^+$ neurodegeneration in the motor cortex and hippocampus, showing respective losses of 11 ± 2.1% ($p = 0.03$) and 15 ± 1.7% ($p = 0.01$) at 7 months and 28 ± 0.9% ($p = 0.001$) and 30 ± 1.2% ($p = 0.001$) at 10 months following injection compared to age-matched vehicle controls (Fig. 3b,c). Similar to LPS-injected mice, motor cortex atrophy preferentially targeted layers I, V, and VI neurons (Fig. 3c) and indiscriminately targeted NeuN$^+$ neurons of the pyramidal layers in the hippocampus. Seven months after DSP-4 injection, the CA1, CA2, and CA3 degenerated by 28 ± 2.1% ($p < 0.001$), 20 ± 3.0% ($p = 0.006$), and 24 ± 3.5% ($p < 0.001$) and by 10 months following exposure had decreased by 45 ± 0.8% ($p < 0.001$), 37 ± 2.2% ($p < 0.001$), and 45 ± 1.4% ($p < 0.001$), respectively (Supplementary Fig. 1). NeuN$^+$ neurons in the caudate/putamen were spared from degeneration even 10 months after DSP-4 injection ($p = 0.12$; Fig. 3b,c).

To confirm that the loss of DA-SN*pc* neurons observed at 10 months following DSP-4 injection represents true neurodegeneration, we co-stained against the pan-neuronal marker NeuN, which confirmed that the 59 ± 4.8% loss of TH$^+$ DA neurons in the SN*pc* ($p < 0.001$) was proportionally reflected by a 52 ± 11.2% loss of NeuN$^+$ neurons ($p = 0.02$; Fig. 4a,b).

DSP-4-elicited neuronal loss in different brain regions was accompanied by a decrease in glucose metabolism measured by PET imaging of [^{18}F]-FDG; levels were reduced in the hindbrain by 24 ± 0.7% ($p = 0.006$), midbrain by 21 ± 0.8% ($p = 0.008$), hippocampus by 23 ± 0.4% ($p = 0.006$), and across all cerebral cortices by 15 ± 0.9% ($p = 0.07$) at 10 months in DSP-4 injected mice compared with vehicle controls (Fig. 3d,e). Furthermore, glucose metabolism was significantly reduced in the olfactory bulb by 18 ± 0.4% ($p = 0.04$) and thalamus by 25 ± 0.9% ($p = 0.009$) implicating putative neurodegeneration in these brain regions. No changes were observed in the cerebellum (−5 ± 0.9%, $p = 0.7$) or the caudate/putamen (4 ± 0.8%, $p = 0.8$; Fig. 3d,e).

DSP-4 Elicits Reactive Microgliosis in Brain Regions Innervated by NE-LC Neurons

Central norepinephrine serves as both a neuromodulator and an anti-inflammatory factor capable of subduing LPS-induced reactive microgliosis [24] by suppressing their release of superoxide, TNFα, IL-1ß, IL-6, iNOS, and other pro-inflammatory factors [24, 35, 36]. We hypothesized that DSP-4-mediated progressive neurodegeneration is likely attributed to the loss of volume transmission signaling from central norepinephrine, which is essential for maintaining microglia quiescence in brain regions innervated by NE-LC neurons. Before investigating whether DSP-4 could induce chronic neuroinflammation, we first verified that DSP-4 is incapable of directly activating microglia in primary neuron-glial cultures (Supplementary Fig. 2a,b). Next, we investigated the spatiotemporal pattern of the microgliosis marker CD11b in different regions throughout the brain following DSP-4 injection. In densitometry assessments found by 7 days following DSP-4 injection, CD11b$^+$ reactive microglia expression was intensified by 90 ± 15.4% in the substantia nigra ($p < 0.001$), 70 ± 6.9% in the motor cortex ($p = 0.001$), and 50 ± 12.2% in the hippocampus ($p = 0.001$), and it peaked at 14 days following injection by 140 ± 12% in the substantia nigra ($p < 0.001$), 130 ± 6.4% in the motor cortex ($p < 0.001$), and 100 ± 20.5% in the hippocampus ($p < 0.001$ Fig. 5a,b). CD11b$^+$ reactive microglia expression remained sustained at these levels at 10 months following DSP-4 injection (Fig. 5a,b). We further performed autoradiography of [^{18}F]-PBR-111 and immunostaining of CD11b$^+$ microglia on the same sections to verify the cell type. Results showed that the increase of uptake of [^{18}F]-PBR-111 correlated well with the activated microglia (Fig. 5c). We also examined whether DSP-4 injection altered microglial morphology into the immunologically activated amoeboid form using the marker Iba-1. Densitometry assessments of Iba-1$^+$ expression on microglia increased significantly at 7 days following DSP-4 injection by 25 ± 3.8% in the substantia nigra ($p = 0.002$), 30 ± 6.6% in the motor cortex ($p = 0.005$), and 25 ± 8.2% in the hippocampus ($p = 0.002$), and it peaked by 14 days following injection by 35 ± 7.8% in the substantia nigra ($p < 0.001$), 35 ± 8.7% in the motor cortex ($p < 0.001$), and 30 ± 10.2% in the hippocampus ($p < 0.001$), where their expression remained stable at these levels for at least 10 months (Supplementary Fig. 3a,b). No significant changes were observed in CD11b$^+$ ($p = 0.2$–0.5; Fig. 5a,b) or Iba-1$^+$ expression ($p = 0.4$–0.9; Supplementary Fig. 3a,b) on microglia in the caudate/putamen.

DSP-4-induced chronic neuroinflammation was functionally assessed by [^{18}F]-PBR-111 PET imaging. At 10 months following DSP-4 injection, neuroinflammation was significantly elevated in the hindbrain by 77 ± 8.5% ($p = 0.02$), the midbrain by 191 ± 9.0% ($p < 0.001$), the hippocampus by 147 ± 8.6% ($p < 0.001$), across all cerebral cortices by 214 ± 10.6% ($p < 0.001$), the thalamus by 380 ± 12.9% ($p < 0.001$), the cerebellum by 90 ± 9.1% ($p = 0.02$), and the olfactory bulb by 49 ± 6.3% ($p = 0.04$) compared to age-matched vehicle controls (Fig. 5d,e). Neuroinflammation in the caudate-putamen remained unchanged (5 ± 1.58%, $p = 0.7$; Fig. 5d,e).

DSP-4-Induced Chronic Neuroinflammation Elevates Oxidative and Nitrosylative Stress in Discrete Neuronal Populations Prior to Their Degeneration

Sustained production of superoxide and other derivative reactive oxygen species (ROS) released by reactive microglia are essential in the maintenance of chronic neuroinflammation and subsequent neurodegeneration. To test whether the progressive neurodegeneration from DSP-4 is attributed to

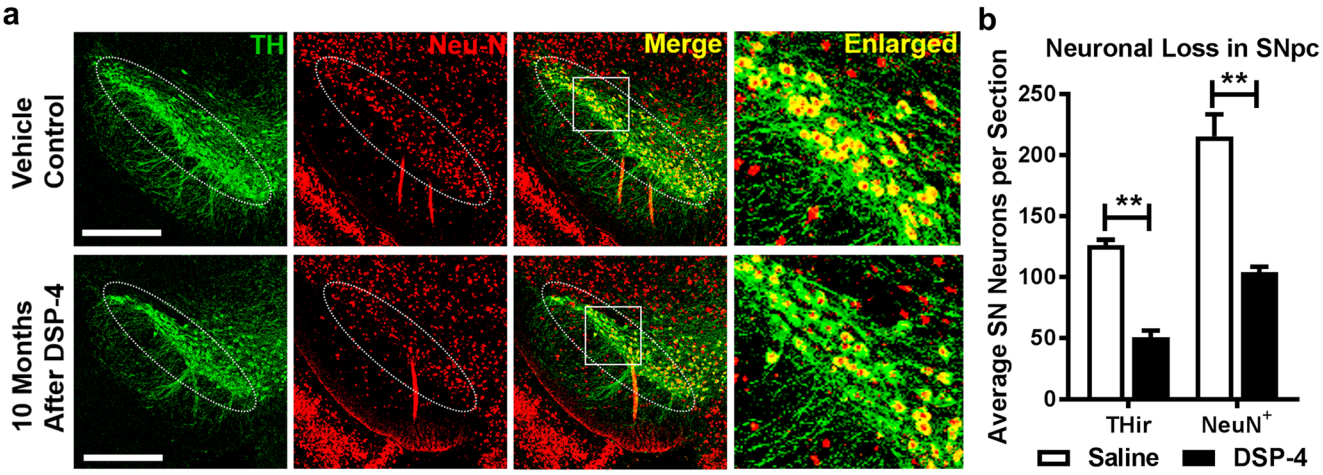

Fig. 4 DSP-4 induced reduction in dopaminergic neuron numbers reflects cell death rather than the downregulation of TH-immunoreactivity. **a** Double immunofluorescent staining of dopaminergic substantia nigra *pars compacta* (DA-SN*pc*) neurons using anti-TH (green) and anti-NeuN (red) antibodies revealed that the decrease of TH^+ DA-SN*pc* neurons at 10 months following DSP-4 was attributed to loss of neurons rather than downregulation of TH^+ expression. The area inside the white box is shown enlarged on the right. Scale bar = 500 μm. **b** $NeuN^+$ neurons in the SNpc were quantified. Results are expressed as a percentage of time-matched DSP-4-treated mice ($n = 5$/group). Data are expressed as mean ± SEM. ** denotes $p < 0.01$

oxidative injuries, we assessed the accumulations of oxidative stress markers in known regions of neurodegeneration. ROS production was visualized in situ by injecting mice with DHE that penetrates the blood-brain barrier and becomes oxidized by superoxide and other forms of ROS into the fluorescent red metabolites 2-hydroxyethidium and ethidium that can be visualized by microscopy. DHE oxidization was significantly increased by 56 ± 9.6% in the substantia nigra ($p = 0.02$), whereas, no obvious changes were found in the hippocampus and motor cortex by 4 months after DSP-4 injection (Fig. 6a,b). At 10 months following DSP-4 injection, DHE oxidization was significantly accumulated by 72 ± 7.4% in the SN ($p < 0.01$), 33 ± 8.8% in the dentate ($p = 0.005$), 24 ± 1.0% in CA1 ($p = 0.008$), 40 ± 7.6% in CA2 ($p = 0.001$), 26 ± 5.7% in CA3 ($p = 0.002$) of the hippocampus, and 46 ± 13.6% ($p = 0.002$) in the motor cortex compared to age-matched controls (Fig. 6a,b).

DSP-4-elicited increase in the production of superoxide/ROS can react with lipid membranes, mitochondria, proteins, and nucleic acids to form both oxidative and nitrosylative products which serve as a marker of inflammation-mediated cell damage. We assessed nitrosylation injuries in DA-SN*pc* neurons by using immunohistochemistry to identify protein nitrosylation through the formation of 3-nitrotyrosine (3-NT) adducts. DSP-4 injection resulted in 855 ± 51.6% increase in 3-NT adduct formation at 10 months following injection compared with age-matched control ($p < 0.001$; Fig. 6c,d). We also performed immunohistochemistry to visualize 4-hydroxy-2-nonenal (HNE) adducts on damaged lipid membranes and found that HNE expression was significantly increased by 528 ± 50% in TH^+ DA-SN*pc* neurons ($p < 0.001$) at 10 months following DSP-4 injection compared to age-matched controls (Fig. 6c,e). Taken together, oxidative and nitrosylative injuries may predict vulnerable neuronal populations at risk of chronic neuroinflammation-driven degeneration.

Suppressing NOX2-Generated Superoxide Following DSP-4-Induced Chronic Neuroinflammation Mitigates Neurodegeneration and Restores Motor Deficits

We have previously reported that addition of norepinephrine to primary neuro-glial cell cultures protects LPS-elicited dopaminergic neurotoxicity through inhibition of microglial NOX2-generated superoxide [24]. To address whether NOX2-derived superoxide in response to DSP-4 exposure is necessary and sufficient to induce progressive neurodegeneration, we injected transgenic mice lacking the catalytic subunit gp91 of NOX2 required for superoxide generation with DSP-4. Baseline microglial densities were not altered in gp91-deficient mice (Fig. 7a) and paired age-matched vehicle controls were evaluated in mice with and without gp91 to account for aging-related changes. Reactive microgliosis, as detected by densitometry analysis of $CD11b^+$ expression, was markedly subdued in the SN, hippocampus, and motor cortex of gp91-deficient mice compared to C57BL/6J mice at 4 months following DSP-4 injection (Fig. 7a,b). Similarly, DSP-4 injection produced a 20% loss of DA-SN*pc* neurons in the C57BL/6J mice ($p = 0.02$), but not in gp91-deficient mice ($p = 0.29$) (Fig. 7c,d).

Though the use of mice with genetic ablations is indispensable for deciphering mechanisms, we also explored whether we could achieve the same findings using a pharmacological NOX2 inhibitor DPI due to its more direct clinical relevance. DPI inhibits superoxide production by irreversibly binding to

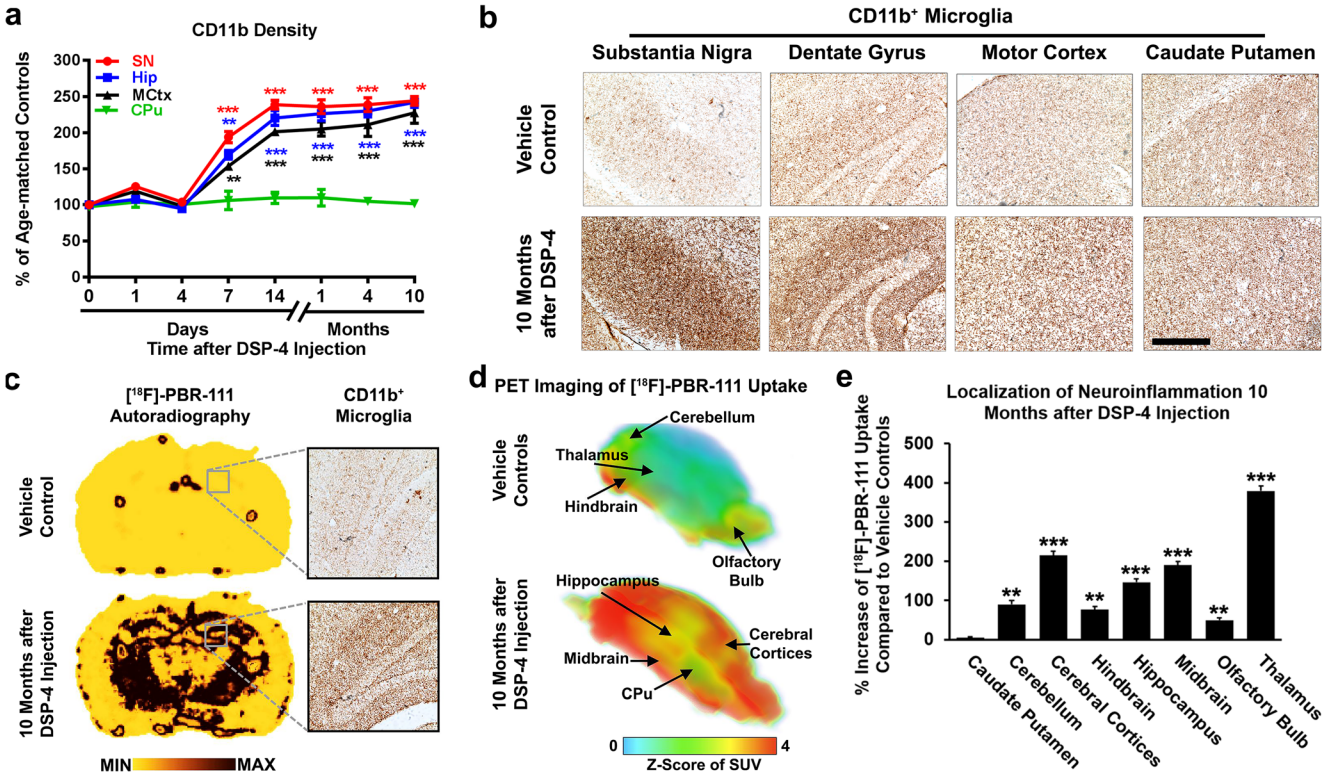

Fig. 5 DSP-4 induces chronic neuroinflammation with heterogeneous densities of microgliosis across several brain regions associated with neurodegeneration in Parkinson's disease. **a** Activation of microglia was assessed by densitometry of CD11b expression in the substantia nigra (SN), hippocampus (Hip), motor cortex (MCtx), and caudate/putamen (CPu) at 1, 4, 7, and 14 days and at 1, 4, and 10 months following an injection of DSP-4 or vehicle to age-matched mice ($n = 4$–6/group). **b** Representative immunostaining images of CD11b$^+$ microglia show significant expression levels associated with reactive microgliosis in the SN, Hip, and MCtx but not the CPu at 10 months following DSP-4 injection. Scale bar = 300 μm. **c** Representative autoradiography of [^{18}F]-PBR-111 uptake corresponds to matching CD11b$^+$ immunostaining images on the same coronal section and confirms that change in radioligand uptake is dependent on microglia density. Age-matched vehicle controls accumulate [^{18}F]-PBR-111 in ventricles, capturing the excretion of the radioligands into the cerebral spinal fluid. **d** In vivo PET imaging of [^{18}F]-PBR-111 uptake is detectable in the olfactory bulb and the hindbrain of age-matched vehicle controls and becomes significant throughout most of the brain with the exception of CPu at 10 months following DSP-4 injection. **e** Quantification of [^{18}F]-PBR-111 uptake is expressed as percentage increase in standard uptake values among different brain regions which was expressed as a percentage increase in uptake following DSP-4 injection compared to vehicle controls. Data are expressed as mean ± SEM. ** denotes $p < 0.01$ and *** $p < 0.001$

the catalytic subunit of gp91^{phox} and when administered at ultralow doses can safely ameliorate DA-SN*pc* neurodegeneration in two models of Parkinson's disease [20]. Mice first received a DSP-4 injection and after a month subcutaneous mini-pumps were implanted, which delivered an ultralow dose of DPI (10 ng/kg/day; s.c.) for 3 months (for the experimental design, see Fig. 8a). Results showed that DPI attenuated DSP-4-induced reactive microgliosis in brain regions innervated by NE-LC neurons. Densitometry analysis of CD11b$^+$ expression by reactive microglia was markedly reduced by 68 ± 12.0% in the substantia nigra ($p = 0.001$), 94 ± 14.2% in the dentate ($p < 0.001$), 85 ± 13.8% in the CA1 ($p = 0.01$), 87 ± 8.7% in the CA2 ($p < 0.001$), 85 ± 10.6 in the CA3 ($p < 0.001$) of the hippocampus, and 77 ± 11.8% in the motor cortex ($p < 0.001$) compared to age-matched mice injected only with DSP-4 (Fig. 8b,c). DSP-4 injection increased the production of superoxide as measured by the amounts of oxidized DHE metabolites by 56 ± 12.1% in the substantia nigra ($p < 0.001$), which was completely reversed by co-infusion with DPI (Fig. 8d,e). DPI also protected TH$^+$ DA-SN*pc* neurons from degeneration at 4 months after DPI injection (36 ± 9.4% loss in the DSP-4 group, 15 ± 16.9% loss in the DPI plus DSP-4 group; Fig. 8f,g). The ability of DPI to rescue DA-SN*pc* neurons from DSP-4-mediated degeneration is also reflected in the restoration of DSP-4-elicited motor deficits as shown in wire hang and rotarod tests in DPI-treated mice (Fig. 8h,i).

Discussion

This study demonstrates that chronic neuroinflammation, induced either by LPS or by DSP-4-elicited depletion of central norepinephrine, is sufficient to induce progressive caudo-rostral degeneration among vulnerable neuronal populations. The spatiotemporal patterns of the neurodegeneration in both mouse models of chronic neuroinflammation approximate the discrete pattern of neurodegeneration [9] and α-synuclein

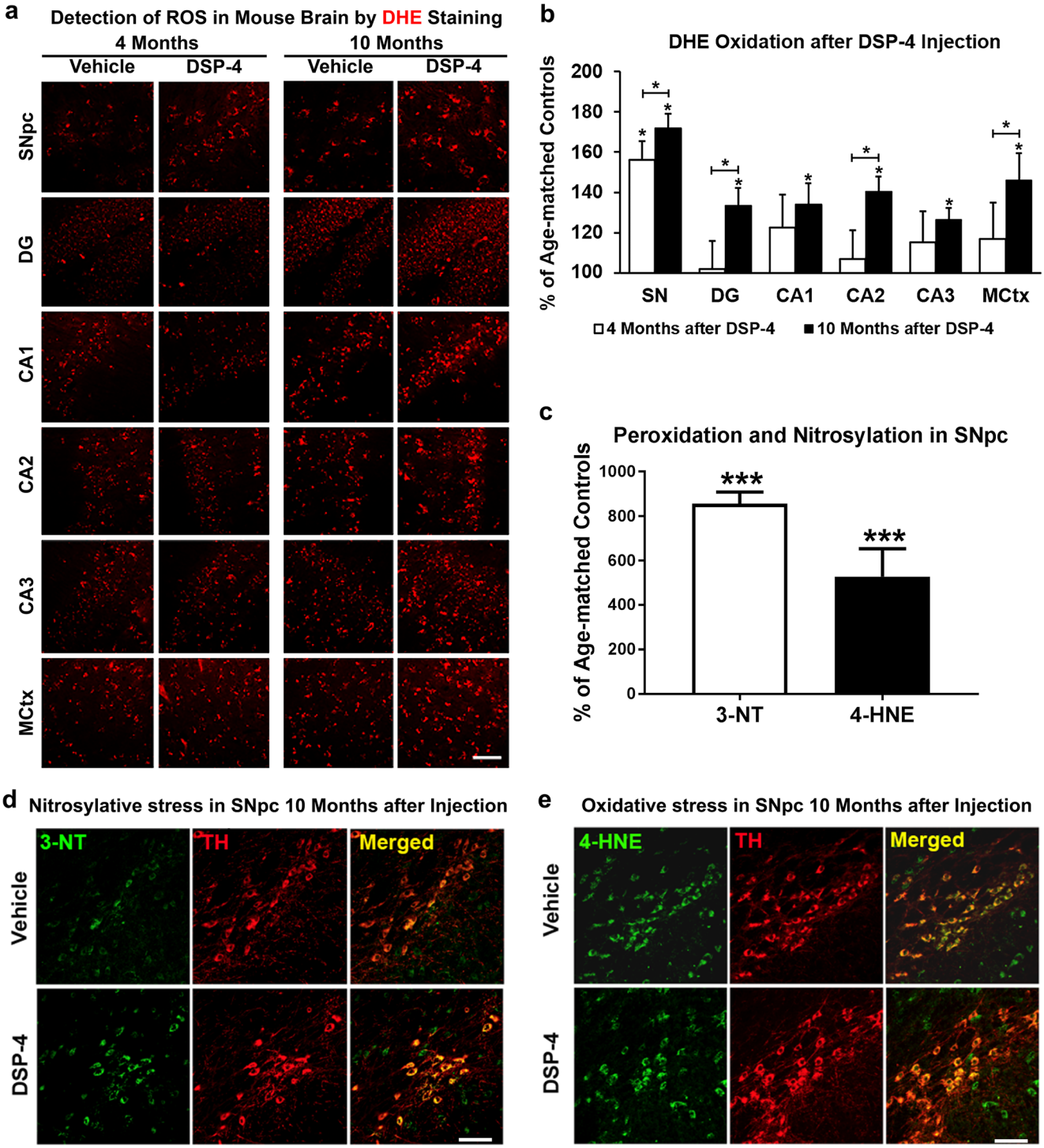

Fig. 6 DSP-4-induced chronic neuroinflammation accumulates oxidative and nitrosylative injuries in vulnerable neurons along the same spatiotemporal pattern of neurodegeneration. **a** DSP-4 injection enhanced red fluorescence intensities indicating increase in production of superoxide/ROS emitted by the oxidized metabolites of DHE following DSP-4 injection compared to age-matched vehicle controls. **b** Densitometry analysis found that DHE significantly accumulates in the SN at 4 months following DSP-4 injection and becomes significantly elevated in the dentate gyrus (DG), CA1, CA2, and CA3 of the hippocampus and motor cortex (MCtx) by 10 months after injection. **c** Densitometry analysis found that DSP-4 injected mice had significantly elevated expression of 3-nitrotyrosine (3-NT) and 4-hydroxynonenal (4-HNE) adducts. **d,e** Enhanced oxidative damage following DSP-4 injection was shown by the increase in both nitrosylation of proteins stained by antibody against 3-NT (**d**) and lipid peroxidation by antibody against 4-HNE (**e**). Data were expressed as the percent increase of DSP-4-exposed mice compared to their age-matched vehicle control ± SEM. * denotes $p < 0.05$, ** $p < 0.01$, and *** $p < 0.001$. Bar = 50 μm. $n = 5–6$

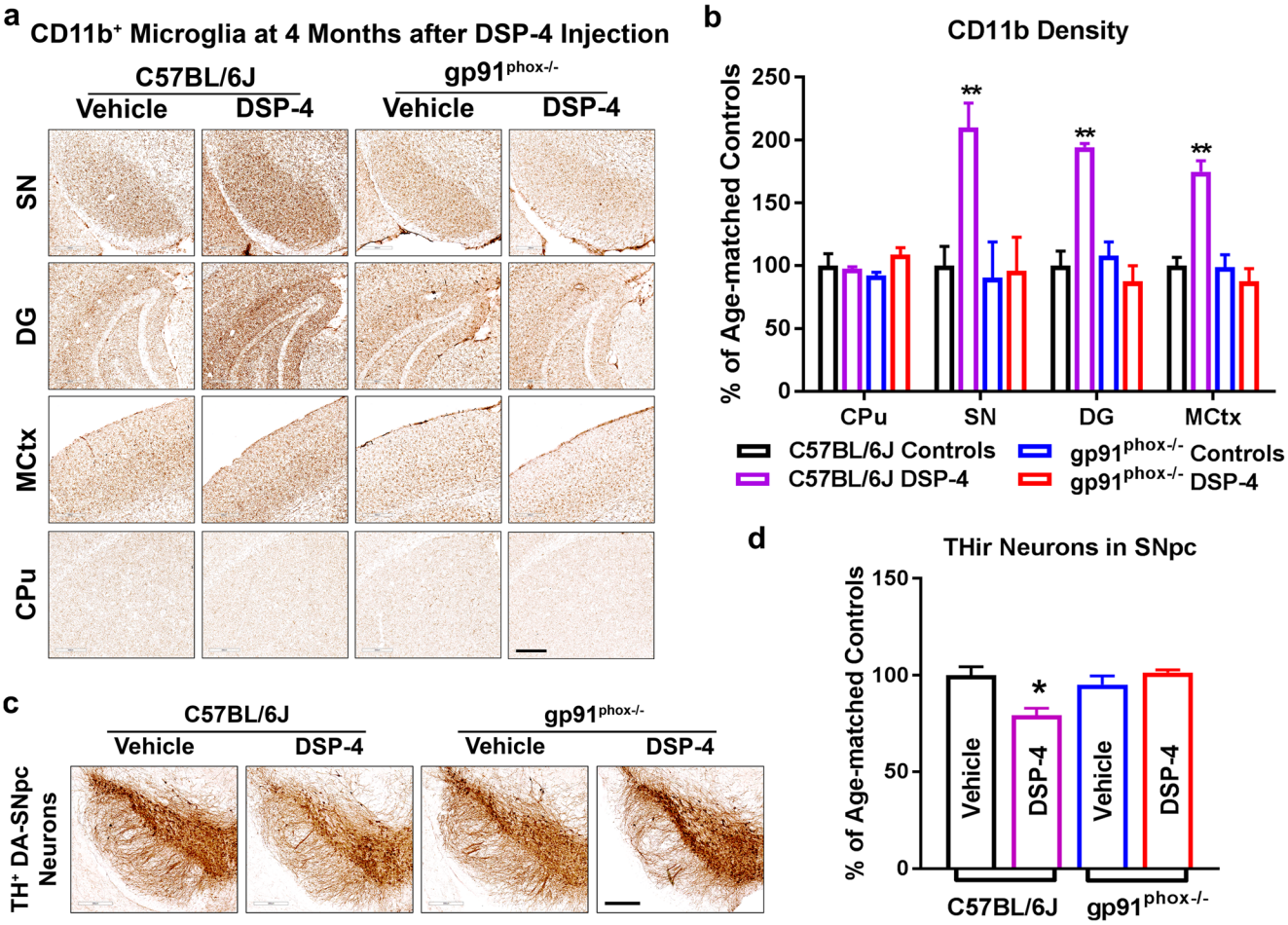

Fig. 7 Genetic ablation of gp91^{phox}, the catalytic subunit of NOX2, abolishes DSP-4-induced reactive microgliosis and DA-SN*pc* neurodegeneration. **a** Assessment of CD11b^{+} reactive microgliosis was performed in the substantia nigra (SN), hippocampus (Hip), motor cortex (MCtx), and caudate/putamen (CPu) of wild-type and gp91$^{phox-/-}$ mice at 4 months following DSP-4 and vehicle injections. **b** Densitometry analysis of CD11b expression found that gp91^{phox}-deficient mice failed to induce reactive microgliosis following exposure to DSP-4. **c**,**d** Ablation of gp91^{phox} rescued TH^{+} DA-SN*pc* neurons from DSP-4-mediated neurodegeneration at 4 months following exposure. Data were expressed as percentage neuronal loss following DSP-4 injection compared to age-matched vehicle controls ($n = 5$/group) ± SEM. * denotes $p < 0.05$ and ** $p < 0.01$. Scale bar = 300 μm

aggregation observed in Parkinson's disease [14]. Mechanistic studies revealed that LPS and DSP-4 produce a similar pattern of chronic neuroinflammation despite differences in chemical structure and mode of actions to activate microglia. Our studies further indicate that prolonged increase in the production of superoxide/ROS is essential for maintaining chronic neuroinflammation in both LPS and DSP-4 models. Chronic neuroinflammation leads to enhanced oxidative and nitrosylative injuries that dictate the temporal order of degeneration observed among different susceptible neuronal populations. Inhibiting NOX2, the key enzyme involved in inflammation-mediated production of superoxide, successfully suppressed chronic neuroinflammation and prevented oxidative neuronal injuries and neurodegeneration following DSP-4 injection. Together, our findings provide strong evidence supporting the idea that the loss of central NE plays a key role in the initiation and maintenance of chronic neuroinflammation and subsequent neurodegenerative process in Parkinson's disease.

Involvement of Chronic Neuroinflammation in Parkinson's Disease

The etiological involvement of chronic neuroinflammation in Parkinson's disease was first proposed several decades ago, and PET imaging studies have since confirmed that Parkinson's disease patients have prominent and heterogeneous neuroinflammation throughout their brains [37, 38]. This study extends our previous findings that LPS-induced chronic neuroinflammation is sufficient not only to produce discrete degeneration of DA-SN*pc* neurons [18, 19, 39] but also to drive the degeneration of other vulnerable neuronal populations outside the basal ganglia in a progressive temporal order similar to that observed in Parkinson's disease.

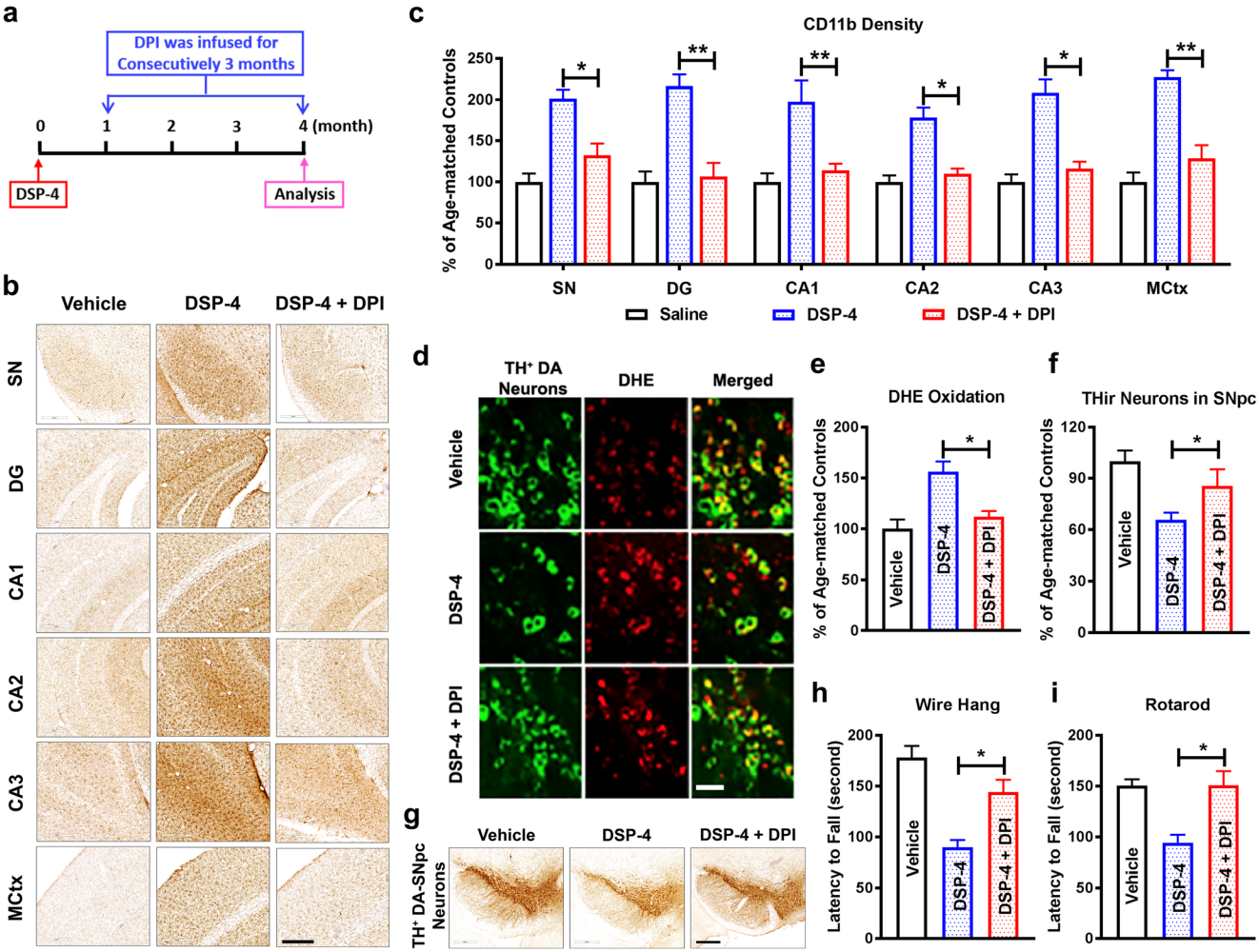

Fig. 8 Post-treatment with a NOX2 inhibitor DPI attenuates DSP-4-induced reactive microgliosis, oxidative stress, DA-SN*pc* neurodegeneration, and motor deficits. **a** Depiction of experimental design, whereby continuous infusion of vehicle or DPI (10 ng/kg/day, s.c.) via osmotic mini-pump was administered one month following DSP-4 injection and maintained for three additional months. **b** DPI treatment significantly suppressed CD11b^{+}-reactive microgliosis in the substantia nigra (SN), dentate gyrus (DG), CA1, CA2, CA3, and motor cortex (MCtx) at 4 months following DSP-4 injection verified by (**c**) densitometry of CD11b expression. **d** DPI treatment suppressed DSP-4-mediated increases in oxidative stress as detected by oxidation of DHE (red) in TH^{+} DA-SN*pc* neurons (green) and confirmed by (**e**) densitometry. **f**,**g** Stereological assessment of TH^{+} DA-SN*pc* neurons found that DPI treatment was sufficient to protect against DSP-4-mediated neurodegeneration ($n = 5$/group). DPI effectively restored DSP-4-induced motor deficits observed in (**h**) wire hang and (**i**) rotarod performance tests ($n = 8$–9/group). Data were expressed as the percent increase in DSP-4-exposed mice compared to their age-matched vehicle control counterparts ± SEM. * denotes $p < 0.05$ and ** $p < 0.01$. Scale = 300 μm

Mechanistically, this systemic LPS injection model generates a sub-lethal septicemia that is capable of immunologically activating the microglia without rupturing the blood-brain barrier, generating a low-grade chronic neuroinflammation for the remaining lifetime of the mouse [18]. The delayed neurodegeneration that occurs in this model implicates that unlike intracranial injection of LPS that result in acute neurodegeneration, chronic neuroinflammation from systemic LPS injection results in a steady release of cytotoxic factors that damage bystander neurons. The re-activation of neighboring microglia through the release of distress factors, such as danger-associated molecular pattern (DAMP), from damaged/dying neurons [40] establishes a self-propelling cycle that eventually results in the irreversible damage and death of neurons that are particularly vulnerable to oxidative damage.

Role of the Loss of Central Norepinephrine in Progressive Neurodegeneration

NE-LC neurons were the most vulnerable to degeneration following LPS-induced chronic neuroinflammation (Fig. 1), likely due to innate features that make them extremely vulnerable to damage from oxidative stress [41, 42]. In Parkinson's disease, central norepinephrine reductions following NE-LC neurodegeneration is primarily associated with the development of several prodromal symptoms [9, 12, 43, 44]. Previous

reports indicate that depletion of central norepinephrine significantly potentiates neuronal lesions in LPS, MPTP, and 6-OHDA Parkinsonian models [24, 36, 45–48]. Conversely, we have previously reported that post-treatment of LPS-injected mice with a ß2-adrenergic receptor agonist salmeterol significantly protects dopaminergic neuron degeneration and prevents motor function deficits [49]. Moreover, asthmatic patients prescribed the ß2-adrenergic receptor agonist salbutamol had reduced lifetime risk of developing Parkinson's disease [50]. These findings suggest that reductions in central norepinephrine may render microglia more prone to over-activation and contribute to the neurodegenerative process in Parkinson's disease. Evidence generated from our DSP-4 study lends strong support to this possibility. Though others have previously reported that norepinephrine disrupts neuro-immune homeostasis [21, 24, 51–53], we are the first to show that a single DSP-4 injection induces permanent chronic neuroinflammation and progressive loss of neurons in several vulnerable brain regions. It is interesting to note that both neuroinflammation and neurodegeneration became persistent even after central norepinephrine levels started to recover (Fig. 3a).

One salient finding of our study was that neurodegeneration in both LPS and DSP-4 chronic neuroinflammation models approximates the spatiotemporal progression observed in Parkinson's disease. Both models show significant DA-SN*pc* neuronal loss a few months following the degeneration of highly vulnerable NE-LC neurons, consistent with the temporal order observed in Parkinson's disease and the sparing of DA neurons in the VTA regions. Furthermore, the numbers of striatal neurons in both LPS- and DSP-4-injected mice were not significantly different from that of saline-injected mice. These findings are similar to the reports indicating, despite clear presence of dendritic degeneration, nonsignificant changes of numbers of medium-spiny neurons that were found in PD patients [31, 32]. Cortical [54, 55] and hippocampal atrophy [56, 57] observed in the late stages of Parkinson's disease occur 10 months following LPS- or DSP-4-induced chronic neuroinflammation. Though microglial densities do seem to differ among the laminar layers of the motor cortex (Figs. 2a, 5b), neurodegeneration was restricted to laminar layers I, V, and VI in both models (Figs. 1a, 3c)—reflecting a topology-dependent susceptibility of pyramidal neurons in these three layers likely due to higher metabolic demands required for long-projection neurotransmission [58]. In line with neurocircuit changes associated with neurodegeneration, both models of chronic neuroinflammation developed behavioral phenotypes that resemble Parkinson's disease symptoms. Fine motor deficits were observed in this (Fig. 8h,i) and previous studies [18], whereas impairments in non-motor phenotypes including anxiety-like behavior, decreased sociability, impaired pre-pulse inhibition to startle, and reduced spatial memory afflicted both LPS- and DSP-4-treated mice [59].

Mechanisms Underlying Chronic Inflammation-Related Spatiotemporal Pattern of Neurodegeneration

In exploring the mechanism that likely drives the discrete spatiotemporal pattern of neurodegeneration following both chronic neuroinflammation models, we speculated that distinct neuronal populations likely respond differently to microenvironments with chronic neuroinflammation and may differentially succumb to oxidative damage associated with aging and Parkinson's disease [60]. The most vulnerable neuronal population seems to share three endogenous features: (1) depleted antioxidant buffering capabilities [61, 62]; (2) greater energetic demands in neurons with long-axon projections or multi-synaptic neurotransmission and pacemaker firing [63, 64]; and (3) are surrounded by high densities of microglia [33, 65]. Following DSP-4-induced chronic neuroinflammation, we found that production of ROS measured by oxidation of DHE and oxidative/nitrosative products, 4-HNE peroxidation and 3-NT nitrosylation adducts were significantly elevated among DA-SN*pc* compared to age-matched vehicle control and far before oxidative injuries appeared in the motor cortex, dentate gyrus, and CA1, CA2, and CA3 neurons of the hippocampus (Fig. 6). Increased production of oxidative radicals led to oxidative injuries that eventually overcome the defensive buffering and cellular repair mechanisms and irreversible damage mitochondria in vulnerable neuronal populations driving bioenergetics failure and cell death [42, 66–69]. Thus, it is likely that the discrete, progressive spatiotemporal patterns of neurodegeneration largely occur in neuronal populations that are vulnerable to oxidative injuries. Consistent with this possibility, we found that in non-injected mice, high basal levels of glucose utilization measured by [^{18}F]-FDG uptake were observed in olfactory bulb, thalamus, and midbrain and hindbrain regions (Figs. 1c,d, 3d,e). We also detected significantly elevated neuroinflammation as detected by [^{18}F]-PBR uptake in the same brain areas after LPS or DSP-4 injection (Figs. 2b,d, 5c–e). These two findings further indicate an intimate relationship between the energy demand and neuronal susceptibility to neuroinflammation and subsequent oxidative injury-related neurodegeneration. Together, these findings strongly suggest that the caudo-rostral order of neurodegeneration may be attributed to an exogenous exposure that generates chronic neuroinflammation and endogenous vulnerability to the oxidative injuries among the degenerating neuronal populations.

NOX2 Is a Key Player in Disease Progression and Prime Target for Development of Disease-Modifying Therapy

Anti-inflammatory therapy has immerged as a disease-modifying strategy for a variety of neurodegenerative diseases

[20, 49, 70–72]. However, the progress of developing efficacious anti-inflammatory therapy for Parkinson's disease has been hampered partly due to the lack of knowledge pinpointing the immune factors released during chronic neuroinflammation. We and others have recently reported that reducing production of superoxide/ROS by targeting both microglial and neuronal NOX2 is an effective strategy to calm neuroinflammation and ameliorate neurodegeneration [20]. We have recently demonstrated that a NOX2 inhibitor DPI in an ultralow dose (10 ng/kg/day; s.c. via mini-pump infusion) exerted potent anti-inflammatory and neuroprotective effects in LPS-injected mice. Post-treatment with DPI in an ultralow dose to LPS-injected mice which has already shown significant loss of nigral dopaminergic neurons and motor deficits could effectively protect the remaining neuronal population and restore motor function [20]. With similar treatment regimens, here, we further established the efficacy of DPI in DSP-4 injected mice. Post-treatment of an ultralow dose of DPI greatly reduced activation of microglia, decreased the production of superoxide/ROS and oxidative products, and most importantly protected SN/DA neuron loss and restored the motor deficits (Fig. 8). The success of using DPI in the DSP-4 model further underlines the importance of targeting the system as future therapeutic strategy for Parkinson's disease patients. Taken together, these studies demonstrated that DPI treatment exerted similar neuroprotective effect in animal models by either infectious agent (LPS) or non-infectious agent (DSP-4) and provided strong evidence suggesting that anti-inflammatory therapy by targeting NOX2 can be an efficacious strategy for Parkinson's disease treatment.

Conclusion

In summary, this study provides strong evidence to further support the idea that chronic neuroinflammation is a critical factor in the progressive neurodegeneration observed in Parkinson's disease. We identified that the loss of central norepinephrine from the degeneration of NE-LC neurons is sufficient to initiate chronic neuroinflammation and drive the progressive and sequential loss of neuronal populations that are vulnerable to oxidative damage. Microglial and neuronal NOX2 is an important regulator of chronic neuroinflammation, and inhibition of this enzyme is sufficient to halt chronic neuroinflammation and oxidative injuries and neurodegeneration among vulnerable neuronal populations and may offer a promising disease-modifying therapeutic strategy for Parkinson's disease.

Acknowledgments This research was supported through the Intramural Research Program at the National Institute of Environmental Health Sciences in the National Institutes of Health, USA. We thank Anthony Lockhart for assistance with animal colony management and maintenance.

Compliance with ethical standards

Disclosures The authors declare that they have no actual or potential competing financial interests.

References

1. Cummings JL (1992) Depression and Parkinson's disease: a review. Am J Psychiatry 149(4):443–454. https://doi.org/10.1176/ajp.149.4.443
2. Remy P, Doder M, Lees A, Turjanski N, Brooks D (2005) Depression in Parkinson's disease: loss of dopamine and noradrenaline innervation in the limbic system. Brain 128(Pt 6):1314–1322. https://doi.org/10.1093/brain/awh445
3. Molano J, Boeve B, Ferman T, Smith G, Parisi J, Dickson D, Knopman D, Graff-Radford N et al (2010) Mild cognitive impairment associated with limbic and neocortical Lewy body disease: a clinicopathological study. Brain 133(Pt 2):540–556. https://doi.org/10.1093/brain/awp280
4. Hanganu A, Bedetti C, Degroot C, Mejia-Constain B, Lafontaine AL, Soland V, Chouinard S, Bruneau MA et al (2014) Mild cognitive impairment is linked with faster rate of cortical thinning in patients with Parkinson's disease longitudinally. Brain 137(Pt 4):1120–1129. https://doi.org/10.1093/brain/awu036
5. Hall H, Reyes S, Landeck N, Bye C, Leanza G, Double K, Thompson L, Halliday G et al (2014) Hippocampal Lewy pathology and cholinergic dysfunction are associated with dementia in Parkinson's disease. Brain 137(Pt 9):2493–2508. https://doi.org/10.1093/brain/awu193
6. Halliday GM, Leverenz JB, Schneider JS, Adler CH (2014) The neurobiological basis of cognitive impairment in Parkinson's disease. Mov Disord 29(5):634–650
7. Baba T, Kikuchi A, Hirayama K, Nishio Y, Hosokai Y, Kanno S, Hasegawa T, Sugeno N et al (2012) Severe olfactory dysfunction is a prodromal symptom of dementia associated with Parkinson's disease: a 3 year longitudinal study. Brain 135(Pt 1):161–169. https://doi.org/10.1093/brain/awr321
8. Arai E, Arai M, Uchiyama T, Higuchi Y, Aoyagi K, Yamanaka Y, Yamamoto T, Nagano O et al (2012) Subthalamic deep brain stimulation can improve gastric emptying in Parkinson's disease. Brain 135(Pt 5):1478–1485. https://doi.org/10.1093/brain/aws086
9. Jellinger KA (1991) Pathology of Parkinson's disease. Changes other than the nigrostriatal pathway. Mol Chem Neuropathol 14(3):153–197
10. Rinne JO, Rummukainen J, Paljarvi L, Rinne UK (1989) Dementia in Parkinson's disease is related to neuronal loss in the medial substantia nigra. Ann Neurol 26(1):47–50. https://doi.org/10.1002/ana.410260107
11. Braak H, Braak E, Yilmazer D, de Vos RA, Jansen EN, Bohl J (1996) Pattern of brain destruction in Parkinson's and Alzheimer's diseases. J Neural Transm (Vienna) 103(4):455–490. https://doi.org/10.1007/BF01276421
12. Zarow C, Lyness SA, Mortimer JA, Chui HC (2003) Neuronal loss is greater in the locus coeruleus than nucleus basalis and substantia nigra in Alzheimer and Parkinson diseases. Arch Neurol 60(3):337–341
13. Buchman AS, Nag S, Shulman JM, Lim AS, VanderHorst VG, Leurgans SE, Schneider JA, Bennett DA (2012) Locus coeruleus neuron density and parkinsonism in older adults without Parkinson's disease. Mov Disord 27(13):1625–1631. https://doi.org/10.1002/mds.25142

14. Braak H, Del Tredici K, Rub U, de Vos RA, Jansen Steur EN, Braak E (2003) Staging of brain pathology related to sporadic Parkinson's disease. Neurobiol Aging 24(2):197–211
15. Gispert S, Del Turco D, Garrett L, Chen A, Bernard DJ, Hamm-Clement J, Korf HW, Deller T et al (2003) Transgenic mice expressing mutant A53T human alpha-synuclein show neuronal dysfunction in the absence of aggregate formation. Mol Cell Neurosci 24(2):419–429
16. Martin LJ, Pan Y, Price AC, Sterling W, Copeland NG, Jenkins NA, Price DL, Lee MK (2006) Parkinson's disease alpha-synuclein transgenic mice develop neuronal mitochondrial degeneration and cell death. J Neurosci 26(1):41–50. https://doi.org/10.1523/JNEUROSCI.4308-05.2006
17. Sacino AN, Brooks M, Thomas MA, McKinney AB, McGarvey NH, Rutherford NJ, Ceballos-Diaz C, Robertson J et al (2014) Amyloidogenic alpha-synuclein seeds do not invariably induce rapid, widespread pathology in mice. Acta Neuropathol 127(5):645–665. https://doi.org/10.1007/s00401-014-1268-0
18. Qin L, Wu X, Block ML, Liu Y, Breese GR, Hong JS, Knapp DJ, Crews FT (2007) Systemic LPS causes chronic neuroinflammation and progressive neurodegeneration. Glia 55(5):453–462. https://doi.org/10.1002/glia.20467
19. Qin LY, Liu YX, Hong JS, Crews FT (2013) NADPH oxidase and aging drive microglial activation, oxidative stress, and dopaminergic neurodegeneration following systemic LPS administration. Glia 61(6):855–868. https://doi.org/10.1002/glia.22479
20. Wang Q, Qian L, Chen SH, Chu CH, Wilson B, Oyarzabal E, Ali S, Robinson B et al (2015) Post-treatment with an ultra-low dose of NADPH oxidase inhibitor diphenyleneiodonium attenuates disease progression in multiple Parkinson's disease models. Brain 138(Pt 5):1247–1262. https://doi.org/10.1093/brain/awv034
21. Dello Russo C, Boullerne AI, Gavrilyuk V, Feinstein DL (2004) Inhibition of microglial inflammatory responses by norepinephrine: effects on nitric oxide and interleukin-1beta production. J Neuroinflammation 1(1):9. https://doi.org/10.1186/1742-2094-1-9
22. Biber K, Neumann H, Inoue K, Boddeke HW (2007) Neuronal 'On' and 'Off' signals control microglia. Trends Neurosci 30(11):596–602. https://doi.org/10.1016/j.tins.2007.08.007
23. Rommelfanger KS, Edwards GL, Freeman KG, Liles LC, Miller GW, Weinshenker D (2007) Norepinephrine loss produces more profound motor deficits than MPTP treatment in mice. Proc Natl Acad Sci U S A 104(34):13804–13809. https://doi.org/10.1073/pnas.0702753104
24. Jiang L, Chen SH, Chu CH, Wang SJ, Oyarzabal E, Wilson B, Sanders V, Xie K et al (2015) A novel role of microglial NADPH oxidase in mediating extra-synaptic function of norepinephrine in regulating brain immune homeostasis. Glia 63(6):1057–1072. https://doi.org/10.1002/glia.22801
25. Cai Z, Chattopadhyay N, Liu WJ, Chan C, Pignol JP, Reilly RM (2011) Optimized digital counting colonies of clonogenic assays using ImageJ software and customized macros: comparison with manual counting. Int J Radiat Biol 87(11):1135–1146. https://doi.org/10.3109/09553002.2011.622033
26. Brooks DJ (2008) Technology insight: imaging neurodegeneration in Parkinson's disease. Nat Clin Pract Neurol 4(5):267–277. https://doi.org/10.1038/ncpneuro0773
27. Mosconi L (2013) Glucose metabolism in normal aging and Alzheimer's disease: methodological and physiological considerations for PET studies. Clin Transl Imaging 1(4):217–233. https://doi.org/10.1007/s40336-013-0026-y
28. Barber TR, Klein JC, Mackay CE, Hu MTM (2017) Neuroimaging in pre-motor Parkinson's disease. Neuroimage Clin 15:215–227. https://doi.org/10.1016/j.nicl.2017.04.011
29. Mirrione MM, Schiffer WK, Fowler JS, Alexoff DL, Dewey SL, Tsirka SE (2007) A novel approach for imaging brain-behavior relationships in mice reveals unexpected metabolic patterns during seizures in the absence of tissue plasminogen activator. Neuroimage 38(1):34–42. https://doi.org/10.1016/j.neuroimage.2007.06.032
30. Gassmann M, Grenacher B, Rohde B, Vogel J (2009) Quantifying Western blots: pitfalls of densitometry. Electrophoresis 30(11):1845–1855. https://doi.org/10.1002/elps.200800720
31. Goto S, Hirano A, Matsumoto S (1990) Immunohistochemical study of the striatal efferents and nigral dopaminergic neurons in parkinsonism-dementia complex on Guam in comparison with those in Parkinson's and Alzheimer's diseases. Ann Neurol 27(5):520–527. https://doi.org/10.1002/ana.410270511
32. Zaja-Milatovic S, Milatovic D, Schantz AM, Zhang J, Montine KS, Samii A, Deutch AY, Montine TJ (2005) Dendritic degeneration in neostriatal medium spiny neurons in Parkinson disease. Neurology 64(3):545–547. https://doi.org/10.1212/01.WNL.0000150591.33787.A4
33. Kim WG, Mohney RP, Wilson B, Jeohn GH, Liu B, Hong JS (2000) Regional difference in susceptibility to lipopolysaccharide-induced neurotoxicity in the rat brain: role of microglia. J Neurosci 20(16):6309–6316
34. Szot P, Miguelez C, White SS, Franklin A, Sikkema C, Wilkinson CW, Ugedo L, Raskind MA (2010) A comprehensive analysis of the effect of DSP4 on the locus coeruleus noradrenergic system in the rat. Neuroscience 166(1):279–291. https://doi.org/10.1016/j.neuroscience.2009.12.027
35. Ignatowski TA, Noble BK, Wright JR, Gorfien JL, Heffner RR, Spengler RN (1997) Neuronal-associated tumor necrosis factor (TNF alpha): its role in noradrenergic functioning and modification of its expression following antidepressant drug administration. J Neuroimmunol 79(1):84–90
36. Heneka MT, Galea E, Gavriluyk V, Dumitrescu-Ozimek L, Daeschner J, O'Banion MK, Weinberg G, Klockgether T et al (2002) Noradrenergic depletion potentiates beta-amyloid-induced cortical inflammation: implications for Alzheimer's disease. J Neurosci 22(7):2434–2442
37. Edison P, Ahmed I, Fan Z, Hinz R, Gelosa G, Ray Chaudhuri K, Walker Z, Turkheimer FE et al (2013) Microglia, amyloid, and glucose metabolism in Parkinson's disease with and without dementia. Neuropsychopharmacol 38(6):938–949. https://doi.org/10.1038/npp.2012.255
38. Brown GC, Neher JJ (2014) Microglial phagocytosis of live neurons. Nat Rev Neurosci 15(4):209–216. https://doi.org/10.1038/nrn3710
39. Gao HM, Zhang F, Zhou H, Kam W, Wilson B, Hong JS (2011) Neuroinflammation and alpha-synuclein dysfunction potentiate each other, driving chronic progression of neurodegeneration in a mouse model of Parkinson's disease. Environ Health Perspect 119(6):807–814. https://doi.org/10.1289/ehp.1003013
40. Chen SH, Oyarzabal EA, Hong JS (2016) Critical role of the Mac1/NOX2 pathway in mediating reactive microgliosis-generated chronic neuroinflammation and progressive neurodegeneration. Curr Opin Pharmacol 26:54–60. https://doi.org/10.1016/j.coph.2015.10.001
41. Elstner M, Muller SK, Leidolt L, Laub C, Krieg L, Schlaudraff F, Liss B, Morris C et al (2011) Neuromelanin, neurotransmitter status and brainstem location determine the differential vulnerability of catecholaminergic neurons to mitochondrial DNA deletions. Mol Brain 4:43. https://doi.org/10.1186/1756-6606-4-43
42. Sanchez-Padilla J, Guzman JN, Ilijic E, Kondapalli J, Galtieri DJ, Yang B, Schieber S, Oertel W et al (2014) Mitochondrial oxidant stress in locus coeruleus is regulated by activity and nitric oxide synthase. Nat Neurosci 17(6):832–840. https://doi.org/10.1038/nn.3717
43. Tong J, Hornykiewicz O, Kish SJ (2006) Inverse relationship between brain noradrenaline level and dopamine loss in Parkinson disease: a possible neuroprotective role for noradrenaline. Arch

Neurol 63(12):1724–1728. https://doi.org/10.1001/archneur.63.12.1724
44. Borodovitsyna O, Flamini M, Chandler D (2017) Noradrenergic modulation of cognition in health and disease. Neural Plast 2017: 6031478:1–14. https://doi.org/10.1155/2017/6031478
45. Lookingland KJ, Chapin DS, McKay DW, Moore KE (1986) Comparative effects of the neurotoxins N-chloroethyl-N-ethyl-2-bromobenzylamine hydrochloride (DSP4) and 6-hydroxydopamine on hypothalamic noradrenergic, dopaminergic and 5-hydroxytryptaminergic neurons in the male rat. Brain Res 365(2):228–234
46. Fornai F, Alessandri MG, Torracca MT, Bassi L, Corsini GU (1997) Effects of noradrenergic lesions on MPTP/MPP+ kinetics and MPTP-induced nigrostriatal dopamine depletions. J Pharmacol Exp Ther 283(1):100–107
47. Perez V, Sosti V, Rubio A, Barbanoj M, Gich I, Rodriguez-Alvarez J, Kulisevsky J (2009) Noradrenergic modulation of the motor response induced by long-term levodopa administration in parkinsonian rats. J Neural Transm (Vienna) 116(7):867–874. https://doi.org/10.1007/s00702-009-0242-9
48. Ostock CY, Lindenbach D, Goldenberg AA, Kampton E, Bishop C (2014) Effects of noradrenergic denervation by anti-DBH-saporin on behavioral responsivity to L-DOPA in the hemi-parkinsonian rat. Behav Brain Res 270:75–85. https://doi.org/10.1016/j.bbr.2014.05.009
49. Qian L, Wu HM, Chen SH, Zhang D, Ali SF, Peterson L, Wilson B, Lu RB et al (2011) Beta 2-adrenergic receptor activation prevents rodent dopaminergic neurotoxicity by inhibiting microglia via a novel signaling pathway. J Immunol 186(7):4443–4454. https://doi.org/10.4049/jimmunol.1002449
50. Mittal S, Bjornevik K, Im DS, Flierl A, Dong X, Locascio JJ, Abo KM, Long E et al (2017) Beta2-adrenoreceptor is a regulator of the alpha-synuclein gene driving risk of Parkinson's disease. Science 357(6354):891–898. https://doi.org/10.1126/science.aaf3934
51. Madrigal JL, Feinstein DL, Dello Russo C (2005) Norepinephrine protects cortical neurons against microglial-induced cell death. J Neurosci Res 81(3):390–396. https://doi.org/10.1002/jnr.20481
52. Heneka MT, Nadrigny F, Regen T, Martinez-Hernandez A, Dumitrescu-Ozimek L, Terwel D, Jardanhazi-Kurutz D, Walter J et al (2010) Locus ceruleus controls Alzheimer's disease pathology by modulating microglial functions through norepinephrine. Proc Natl Acad Sci U S A 107(13):6058–6063. https://doi.org/10.1073/pnas.0909586107
53. Gyoneva S, Traynelis SF (2013) Norepinephrine modulates the motility of resting and activated microglia via different adrenergic receptors. J Biol Chem 288(21):15291–15302. https://doi.org/10.1074/jbc.M113.458901
54. Hilker R, Thomas AV, Klein JC, Weisenbach S, Kalbe E, Burghaus L, Jacobs AH, Herholz K et al (2005) Dementia in Parkinson disease: functional imaging of cholinergic and dopaminergic pathways. Neurology 65(11):1716–1722. https://doi.org/10.1212/01.wnl.0000191154.78131.f6
55. Braak H, Rub U, Gai WP, Del Tredici K (2003) Idiopathic Parkinson's disease: possible routes by which vulnerable neuronal types may be subject to neuroinvasion by an unknown pathogen. J Neural Transm 110(5):517–536. https://doi.org/10.1007/s00702-002-0808-2
56. Dickson DW, Schmidt ML, Lee VM, Zhao ML, Yen SH, Trojanowski JQ (1994) Immunoreactivity profile of hippocampal CA2/3 neurites in diffuse Lewy body disease. Acta Neuropathol 87(3):269–276
57. Pereira JB, Junque C, Bartres-Faz D, Ramirez-Ruiz B, Marti MJ, Tolosa E (2013) Regional vulnerability of hippocampal subfields and memory deficits in Parkinson's disease. Hippocampus 23(8): 720–728. https://doi.org/10.1002/hipo.22131
58. Parent M, Parent A (2006) Relationship between axonal collateralization and neuronal degeneration in basal ganglia. J Neural Transm Suppl 70:85–88
59. Song S, Chen SH, Moy S, Wang QS, Hong JS (2017) Norepinephrine deficiency accelerates ascending sequential neurodegeneration and progression of non-motor/motor symptoms in an inflammatory Parkinson's diseases mouse model. In: Society for neuroscience annual meeting, Washington D.C.
60. Sanders LH, Greenamyre JT (2013) Oxidative damage to macromolecules in human Parkinson disease and the rotenone model. Free Radic Biol Med 62:111–120. https://doi.org/10.1016/j.freeradbiomed.2013.01.003
61. Wang X, Michaelis EK (2010) Selective neuronal vulnerability to oxidative stress in the brain. Front Aging Neurosci 2(12). https://doi.org/10.3389/fnagi.2010.00012
62. Smeyne M, Smeyne RJ (2013) Glutathione metabolism and Parkinson's disease. Free Radic Biol Med 62:13–25. https://doi.org/10.1016/j.freeradbiomed.2013.05.001
63. Surmeier DJ, Obeso JA, Halliday GM (2017) Selective neuronal vulnerability in Parkinson disease. Nat Rev Neurosci 18(2):101–113. https://doi.org/10.1038/nrn.2016.178
64. Surmeier DJ, Schumacker PT (2013) Calcium, bioenergetics, and neuronal vulnerability in Parkinson's disease. J Biol Chem 288(15): 10736–10741. https://doi.org/10.1074/jbc.R112.410530
65. Yang TT, Lin C, Hsu CT, Wang TF, Ke FY, Kuo YM (2013) Differential distribution and activation of microglia in the brain of male C57BL/6J mice. Brain Struct Funct 218(4):1051–1060. https://doi.org/10.1007/s00429-012-0446-x
66. Guzman JN, Sanchez-Padilla J, Wokosin D, Kondapalli J, Ilijic E, Schumacker PT, Surmeier DJ (2010) Oxidant stress evoked by pacemaking in dopaminergic neurons is attenuated by DJ-1. Nature 468(7324):696–U119. https://doi.org/10.1038/nature09536
67. Surmeier DJ, Guzman JN, Sanchez-Padilla J, Schumacker PT (2011) The role of calcium and mitochondrial oxidant stress in the loss of substantia nigra pars compacta dopaminergic neurons in Parkinson's disease. Neuroscience 198:221–231. https://doi.org/10.1016/j.neuroscience.2011.08.045
68. Goldberg JA, Guzman JN, Estep CM, Ilijic E, Kondapalli J, Sanchez-Padilla J, Surmeier DJ (2012) Calcium entry induces mitochondrial oxidant stress in vagal neurons at risk in Parkinson's disease. Nat Neurosci 15(10):1414–1421. https://doi.org/10.1038/nn.3209
69. Burbulla LF, Song P, Mazzulli JR, Zampese E, Wong YC, Jeon S, Santos DP, Blanz J et al (2017) Dopamine oxidation mediates mitochondrial and lysosomal dysfunction in Parkinson's disease. Science 357(6357):1255–1261. https://doi.org/10.1126/science.aam9080
70. Wyss-Coray T, Mucke L (2002) Inflammation in neurodegenerative disease—a double-edged sword. Neuron 35(3):419–432
71. Gilgun-Sherki Y, Melamed E, Offen D (2006) Anti-inflammatory drugs in the treatment of neurodegenerative diseases: current state. Curr Pharm Des 12(27):3509–3519
72. Liu B, Jiang JW, Wilson BC, Du L, Yang SN, Wang JY, Wu GC, Cao XD et al (2000) Systemic infusion of naloxone reduces degeneration of rat substantia nigral dopaminergic neurons induced by intranigral injection of lipopolysaccharide. J Pharmacol Exp Ther 295(1):125–132